Available online at www.sciencedirect.com
ScienceDirect
Acta Materialia 56 (2008) 1546–1554
Acta MATERIALIA
www.elsevier.com/locate/actamat

Self-consistent scale transition with imperfect interfaces: Application to nanocrystalline materials

L. Capolungo [a,b,*], S. Benkassem [c], M. Cherkaoui [a,b], J. Qu [a,b]

[a] UMI 2958 GT-CNRS, Metz 57000, France
[b] George W. Woodruff School of Mechanical Engineering, Atlanta, GA 30332-0405, USA
[c] LPMM-CNRS Université Paul Verlaine, Ile du Saulcy, 57045 Metz Cedex 1, France

Received 21 August 2007; received in revised form 28 November 2007; accepted 4 December 2007
Available online 20 February 2008

Abstract

A hierarchal scale transition technique is introduced to model the effect of imperfect interfaces on the elastoviscoplastic response of composite materials. This novel framework is based on a two-step procedure. In the first step, an inclusion is embedded in a matrix phase and the interface between the two phases is imperfect. The embedded inclusion is homogenized via the use of a Mori–Tanaka scheme. In a second step the homogenized inclusion is introduced in a matrix phase representing the homogeneous equivalent material, and the macroscopic response of the material is obtained via the self-consistent approximation. The model is applied to the case of pure nanocrystalline copper and allows the activity of grain boundary sliding to be quantified.

Keywords: Micromechanics; Interface; Nanocrystalline; Grain boundary sliding

1. Introduction

The strength, ductility and cyclic response of multiphased materials are dependent on the individual response of each material's constituents, and on the interaction between each phase. The predominant effect of such interaction is localized along the interfaces between each phase.

Such interface effects are of great interest in the case of nanostructured materials which typically exhibit a large volume-to-interface ratio. This is particularly the case for nanocrystalline materials with grain sizes smaller than ~30 nm for which the volume fraction of grain boundaries, which constitutes an interphase between two crystals, is as high as 50% [1]. Also, as exhibited in transmission electron microscopy experiments and quasi-continuum simulations on bicrystal interfaces, the grain boundary/grain interior interface is typically imperfect and leads to a relative motion of the two phases across the interface [2,3]. Therefore, appropriate modeling of the response of composite materials, and nanostructured materials in particular, will account for the effect of imperfect interfaces.

The deformation mechanisms arising from the presence of imperfect interfaces, and the formalisms allowing the description of such interfaces, have been particularly investigated in the case of the creep response of polycrystalline materials. Zener studied the effect of viscous grain boundaries on the elastic properties of isotropic polycrystals by considering the relative motion of grain boundaries as a shear stress relaxation process [4]. This model, applicable at high temperatures and in the elastic regime, does not describe the mechanisms – and their activation criteria – by which grains slide relative to one another. Langdon proposed a non-Newtonian viscous law that was valid in the steady-state regime and that accounted for the effect of the thermally activated mechanism of dislocation glide and climb along the grain boundary [5]. This model was

* Corresponding author. Address: George W. Woodruff School of Mechanical Engineering, Atlanta, GA 30332-0405, USA. Tel.: +1 5054120723.
E-mail address: laurentc@lanl.gov (L. Capolungo).

1359-6454/$34.00
doi:10.1016/j.actamat.2007.12.018

later extended by Wu and Koul to account for the effect of grain boundary precipitates [6,7]. Alternatively, Raj and Ashby proposed a model for grain boundary sliding in which the relative displacement of two crystals separated by a non-planar interface is driven by steady-state vacancy diffusion [8]. Mori and co-workers investigated the interrelations between diffusion accommodated and non-accommodated grain boundary sliding [9,10]. The proposed framework is based on a hierarchal scale transition where the displacement jumps at the interfaces, referred to as Somigliana's dislocations, are separated into a normal contribution and a tangential contribution. The former arises from steady-state diffusion while the latter arises from non-accommodated grain boundary sliding described by a Newtonian viscous law.

The above-mentioned models were developed to describe the creep response of polycrystalline materials. In the case of the quasi-static response of polycrystalline materials, it was suggested in a recent quasi-continuum study that grain boundary sliding may be described as a stick–slip mechanism [3].

In terms of length scale, the interface needs to be described at the length scale of the microstructure, and the macroscopic effect of imperfect interface bonding can be extracted from the use of a scale transition technique. For example, Wei and Anand [11] introduced a numerical model for the effect of imperfect interfaces on the response of nanocrystalline materials in which the scale transition is performed via the used of the finite element method. Similarly, the scale transition could be performed via the use of continuum micromechanics [9].

In this work, a hierarchal micromechanical scheme accounting for the effect of imperfect interfaces is introduced. The model is developed for the case of two-phase materials and could be extended to the case of n-phase materials. The scale transition is based on the following procedure. First, the material is represented as a two-phase material composed of an inclusion phase (phase 1) embedded in a matrix phase (phase 2). The interface between the two phases is assumed imperfect and the homogenized viscoplastic response of the embedded inclusion is obtained via the used of a Mori–Tanaka scheme [12]. Second, the homogenized inclusion (HI) is embedded in a second matrix phase representing the homogeneously equivalent material (HEM) and the macroscopic response of the material in the viscoplastic regime, is obtained via the self-consistent approximation. In this second step, the interface between the HI and HEM is assumed perfect. The solution to the elastoviscoplastic problem is obtained via the field translation method introduced in work by Sabar et al. [14] and Berbenni et al. [13]. The model is applied to the case of pure nanocrystalline copper using the behavior of grain interiors and grain boundaries described previously by the authors [15–17]. As a first approach, the imperfect interface is described via the introduction of a law accounting for the activity of stick–slip sliding discussed in Warner et al.'s model [3].

2. Scale transition framework

Considering a two-phase composite material with imperfect interfaces, the material can be equivalently represented as an inclusion embedded in a matrix phase or, as introduced in work by Christensen and Lo [18], as a three-phase material composed of a coated inclusion embedded in a matrix phase. The former leads to a relatively simple expression for the localization relations while the latter typically leads to softer predictions of the overall material response. On the one hand, it was shown that three-phase models more adequately account for interface effects [19]. Note that these scale transition techniques based on three-phase representations of the materials require the introduction of interfacial operators [20]. In the case of perfect mobile interfaces, these can be obtained by using Hadamard compatibility conditions [19,21]; however, to the authors' knowledge, no closed-form expressions of the interfacial operators exist in the case of imperfect interfaces. On the other hand, it was shown in early work by Qu [22,23] that the effect of slightly more compliant interfaces on the elastic response of two-phase composite materials can be accounted for via the use of a two-phase representation. Therefore the idea is to decompose an initially three-phase problem into two two-phase problems. Precisely stated, the first problem considered is that of an inclusion, representing phase 1, embedded in a matrix phase representing phase 2. The interface between phases 1 and 2 is imperfect. The homogenized response of problem 1 is obtained via the use of the Mori–Tanaka scheme. It is then introduced into a second problem composed of the HI introduced into the HEM; the macroscopic response of the material in the viscoplastic regime is subsequently obtained via the self-consistent approximation. The overall elastoviscoplastic response of the composite material is obtained via the field translation method [14]. A schematic of the proposed framework is presented in Fig. 1.

Prior to solving the problem of embedded inclusions with imperfect interfaces in the case of elasticviscoplastic behaviors, let us treat the case of pure viscoplastic behaviors. As mentioned in the above, the problem is treated in two steps as presented in Fig. 2. First, the discontinuity between the inclusion and the coating will be treated. This interface is not perfect and allows relative sliding of the inclusion with respect to the matrix. The behavior of the homogenized inclusion will be extracted from the application of a Mori–Tanaka scheme [12]. Second, the homogeneous medium/homogeneous inclusion discontinuity is treated. In this case the interface is perfect. Linking the solutions of steps 1 and 2 will lead to the desired expression of the localization relation. However, let us note here that the inclusion/matrix relation is clearly approximated in this approach.

The following notations will be used; the superscripts vp, I, M, HI and e will refer to a viscoplastic term, to the inclusion phase, to the matrix phase, to the homogenized inclusion and to the effective material, respectively. Tensors will be written in bold characters and their components will be

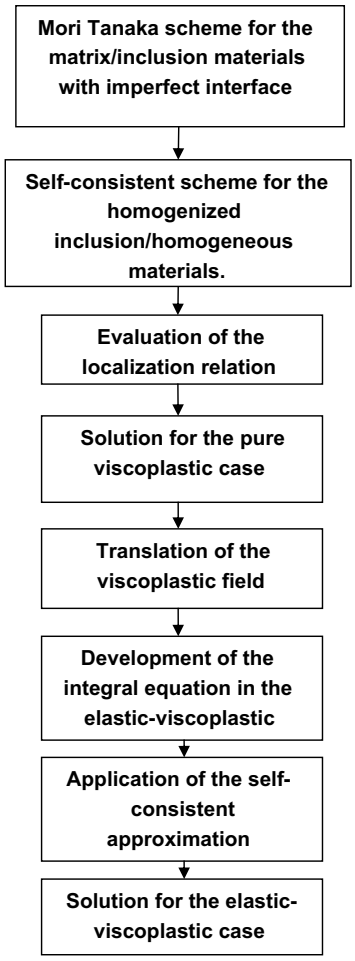

Fig. 1. Schematic of the scale transition procedure.

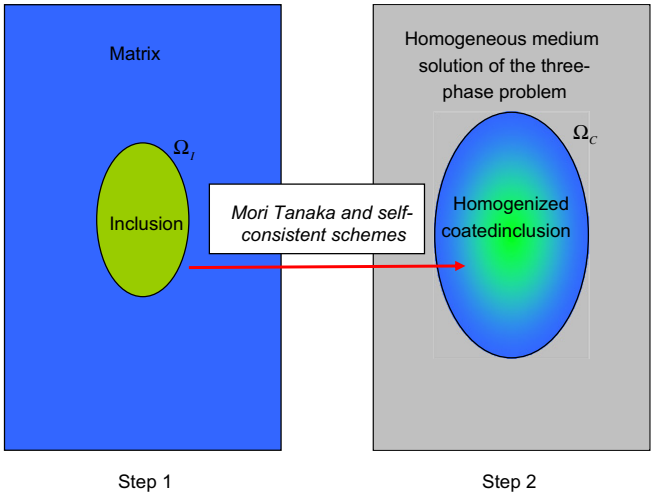

Fig. 2. Schematic of the two steps used to solve the three-phase viscoplastic problem.

denoted with subscripts $i, j, k, l, m, n = 1, 2, 3$. Also, $\boldsymbol{B}^*$ (with $^* = $ vpI, vpM, vpHI) will refer to viscoplastic localization tensor and $\boldsymbol{b}^*$ (with $^* = $ I, M, HI) will refer to viscosity tensors. The symbol : will refer to the double dot product.

Finally, for the sake of brevity, the localization expression will be given solely with respect to the inclusion phase. However, the equivalent localization expressions in the case of the matrix phase are found simply from the macro-homogeneity condition which sets the volume average of the localization tensors equal to the identity tensor.

Let us first discuss the solution of step 1. For the sake of clarity let us recall that the problem to be solved corresponds to the case of a two-phase material composed of an inclusion phase embedded in a matrix phase. Also, in this case the inclusion/matrix interface is not perfect. Across the interface the traction vector remains continuous:

$$\Delta\boldsymbol{\sigma}_{ij}\boldsymbol{n}_j \equiv [\boldsymbol{\sigma}_{ij}(S^+) - \boldsymbol{\sigma}_{ij}(S^-)]\boldsymbol{n}_j = 0 \text{ with } i, j = 1, 2, 3. \quad (1)$$

Here the superscripts + and − denote the respective positive and negative sides of the interface denoted S. $\boldsymbol{n}$ denotes the vector normal to the interface. $\boldsymbol{\sigma}$ denotes the Cauchy stress tensor and the symbol Δ denotes a jump across the interface. As a first approach, the jump condition across the interface is given here in a manner similar to that proposed by Qu [22] and relates the jump in the displacement, denoted $\boldsymbol{u}$, to the stress at the interface with a tensor $\boldsymbol{\eta}$:

$$\Delta\boldsymbol{u}_i \equiv \boldsymbol{u}_i(S^+) - \boldsymbol{u}_i(S^-) = \boldsymbol{\eta}_{ij}\boldsymbol{\sigma}_{jk}\boldsymbol{n}_k. \quad (2)$$

Here $\boldsymbol{\eta}_{ij}$ represents the compliance of the interface and is given by

$$\boldsymbol{\eta}_{ij} = \alpha\delta_{ij} + (\beta - \alpha)\boldsymbol{n}_i\boldsymbol{n}_j. \quad (3)$$

For the sake of illustration, a sliding law describing the mechanism of stick–slip is proposed. α is given by the following formula:

$$\alpha = \frac{\delta_c}{\boldsymbol{\sigma}_c\left(1 - \frac{\sum_i \Delta\boldsymbol{u}_i}{\delta_c}\right)}. \quad (4)$$

Here δ_c and $\boldsymbol{\sigma}_c$ denote a critical distance and a critical stress, respectively. This expression corresponds to the converse of that proposed by Warner et al. [3] for the description of the stick–slip mechanism. Since void creation is not accounted for in this study β is set to zero. Let us recall that the stick–slip mechanism corresponds to the alternate bonding and debonding of the group of atoms delimiting the interface. From Eq. (4), it can be seen that, until the sum of the displacement jump reaches a critical relative displacement δ_c, an increase in the sum of the displacement jump leads to an increase in α. This would correspond to the debonding of the group of atoms composing the interface. Also, α should drop sharply when the sum of the displacement jump reaches δ_c, which is the limiting value. This would correspond to the creation of new atomic bonds. Finally, let us note that as opposed to Onaka's work [10], the present model is not restricted to a constant interface compliance.

Note here that the model could be extended to different interface behaviors. For example, as discussed elsewhere [22], the free sliding case can be studied by setting β to zero

and α to infinity. With the above-mentioned representative element, the typical expression of Navier's equations – which results from the consecutive use of the compatibility and equilibrium conditions – can be obtained

$$\boldsymbol{b}^{C}_{ijkl}\dot{\boldsymbol{u}}_{k,lj}(x) - (\boldsymbol{b}^{C}_{ijkl} - \boldsymbol{b}_{ijkl}(x))\dot{\boldsymbol{\varepsilon}}^{\mathrm{vp}}_{kl,j}(x) = 0. \tag{5}$$

Here, x, $\boldsymbol{b}^{C}$, $\boldsymbol{b}$, $\dot{\boldsymbol{u}}$, and $\dot{\boldsymbol{\varepsilon}}^{\mathrm{vp}}$ denote the position, the viscosity tensor within the matrix phase, the local viscosity tensor, the displacement rate and the local strain rate, respectively. Also, at any point x the displacement engendered by a unit force at point x' must respect the following:

$$\boldsymbol{b}^{C}_{ijlk}\frac{\partial^2 \boldsymbol{G}^{\infty}_{km}(x,x')}{\partial x_l \partial x_j} + \delta_{im}\delta(x-x') = 0 \text{ with } i,j,k,l,m = 1,2,3. \tag{6}$$

Here $\boldsymbol{G}^{\infty}$, δ and $\delta(x-x')$ denote Green's function, Kronecker's delta and the Dirac function, respectively. The symbol $\partial/\partial x$ denotes a partial derivative. Integrating the following equation on a volume, denoted Ω, and multiplying the resulting equation by the displacement rate vector, $\dot{\boldsymbol{u}}$, leads to the following expression:

$$\int_{\Omega}\dot{\boldsymbol{u}}_i(x)\boldsymbol{b}^{\mathrm{M}}_{ijkl}\frac{\partial^2 \boldsymbol{G}^{\infty}_{km}(x,x')}{\partial x_l \partial x_j}\,\mathrm{d}\Omega(r) = \begin{cases} -\dot{\boldsymbol{u}}_m(x') & x' \in \Omega \\ 0 & x' \notin \Omega \end{cases} \tag{7}$$

Using the divergence theorem, one can rewrite the volume integral in Eq. (7) as follows:

$$\begin{aligned}\int_{\Omega}\dot{\boldsymbol{u}}_i(x)\boldsymbol{b}^{\mathrm{M}}_{ijkl}\frac{\partial^2 \boldsymbol{G}_{km}(x,x')}{\partial x_l \partial x_j}\,\mathrm{d}\Omega(x) &= \int_{S}\dot{\boldsymbol{u}}_i(x)\boldsymbol{b}^{\mathrm{M}}_{ijkl}\frac{\partial \boldsymbol{G}_{km}(x,x')}{\partial x_l}\boldsymbol{n}_j\,\mathrm{d}S(x) \\ &\quad - \int_{V}\dot{\boldsymbol{u}}_{i,j}(x)\boldsymbol{b}^{\mathrm{M}}_{ijkl}\frac{\partial \boldsymbol{G}_{km}(x,x')}{\partial x_l}\,\mathrm{d}\Omega(x)\end{aligned} \tag{8}$$

where S denotes the surface surrounding Ω, and $\boldsymbol{n}_i$ denotes the unit outward normal. Furthermore, multiplying Navier's equation (5) by Green's function and integrating the resulting expression on the same volume Ω leads to the following expression:

$$\int_{\Omega}\boldsymbol{G}^{\infty}_{im}(x,x')\boldsymbol{b}^{\mathrm{M}}_{ijkl}\dot{\boldsymbol{u}}_{k,lj}(x)\mathrm{d}\Omega(x) - \int_{\Omega}\boldsymbol{G}^{\infty}_{im}(x,x')\left(\boldsymbol{b}^{\mathrm{M}}_{ijkl} - \boldsymbol{b}^{\mathrm{I}}_{ijkl}\right)\dot{\boldsymbol{\varepsilon}}^{\mathrm{vp}}_{kl,j}(x)\mathrm{d}\Omega(x) = 0. \tag{9}$$

Subtracting (8) from (9) and using the divergence theorem, one obtains

$$\begin{aligned}&\int_{S}\boldsymbol{b}^{\mathrm{M}}_{ijkl}\left(\boldsymbol{G}^{\infty}_{im}(x,x')\left(\dot{\boldsymbol{u}}_{k,l}(x) - \left(I_{klmn} - \left(\boldsymbol{b}^{\mathrm{M}}_{klpq}\right)^{-1}\boldsymbol{b}_{pqmn}\right)\dot{\boldsymbol{\varepsilon}}^{\mathrm{vp}}_{mn}(x)\right)\right. \\ &\left.-\dot{\boldsymbol{u}}_i(x)\frac{\partial \boldsymbol{G}_{km}(x,x')}{\partial x_l}\right)\boldsymbol{n}_j\,\mathrm{d}S(x) \\ &+\int_{\Omega}\frac{\partial \boldsymbol{G}^{\infty}_{im}(x,x')}{\partial x_l}\left(\boldsymbol{b}^{\mathrm{M}}_{ijkl} - \boldsymbol{b}_{ijkl}\right)\dot{\boldsymbol{\varepsilon}}^{\mathrm{vp}}_{kl}(x)\mathrm{d}\Omega(x) = \begin{cases}\dot{\boldsymbol{u}}_m x' & x' \in \Omega \\ 0 & x' \notin \Omega\end{cases}\end{aligned} \tag{10}$$

Supposing the arbitrary volume to represent the inclusion's volume, denoted Ω_{I}, Eq. (10) can be simplified by virtue of local considerations. Therefore, when r' belongs to the inclusion, the constitutive relation can be identified within the above expression and Eq. (10) becomes

$$\begin{aligned}\dot{\boldsymbol{u}}_m(x') = &\int_{S^-}\left(\boldsymbol{G}^{\infty}_{im}(x,x')\boldsymbol{\sigma}_{kl} - \boldsymbol{b}^{\mathrm{M}}_{ijkl}\dot{\boldsymbol{u}}_i(x)\frac{\partial \boldsymbol{G}_{km}(x,x')}{\partial x_l}\right)\boldsymbol{n}_j\,\mathrm{d}S(x) \\ &+\int_{\Omega_I}\frac{\partial \boldsymbol{G}^{\infty}_{im}(x,x')}{\partial x_l}\left(\boldsymbol{b}^{\mathrm{M}}_{ijkl} - \boldsymbol{b}_{ijkl}\right)\dot{\boldsymbol{\varepsilon}}^{\mathrm{vp}}_{kl}(x)\mathrm{d}\Omega_{\mathrm{I}}(x)\end{aligned} \tag{11}$$

Similarly, in the case where x' is exterior to Ω_{I}, one obtains the following relation:

$$0 = \int_{S^+}\left(\boldsymbol{G}^{\infty}_{im}(x,x')\boldsymbol{\sigma}_{kl} - \boldsymbol{b}^{\mathrm{M}}_{ijkl}\dot{\boldsymbol{u}}_i(x)\frac{\partial \boldsymbol{G}_{km}(x,x')}{\partial x_l}\right)\boldsymbol{n}_j\,\mathrm{d}S(x) \tag{12}$$

Subtracting (11) from (12), one obtains the expression of the displacement rate at any point within the representative element:

$$\begin{aligned}\dot{\boldsymbol{u}}_m(r) = &\int_{S}\left(\boldsymbol{b}^{\mathrm{M}}_{ijkl}\Delta\dot{\boldsymbol{u}}_i(x')\frac{\partial \boldsymbol{G}_{km}(x,x')}{\partial x_l}\right)\boldsymbol{n}_j\,\mathrm{d}S(x') \\ &+\int_{\Omega_{\mathrm{I}}}\frac{\partial \boldsymbol{G}^{\infty}_{im}(x,x')}{\partial x_l}\left(\boldsymbol{b}^{\mathrm{M}}_{ijkl} - \boldsymbol{b}_{ijkl}\right)\dot{\boldsymbol{\varepsilon}}^{\mathrm{vp}}_{kl}(x')\mathrm{d}V(x')\end{aligned} \tag{13}$$

Let us note that the jump in the displacement rate is introduced in Eq. (13). Differentiating the above expression and supposing homogeneity of the strain rate tensor within the inclusion, one obtains

$$\begin{aligned}\dot{\boldsymbol{u}}_{m,n}(x) = &\int_{S}\left(\boldsymbol{b}^{\mathrm{M}}_{ijkl}\Delta\dot{\boldsymbol{u}}_i(x')\frac{\partial \boldsymbol{G}_{km}(x,x')}{\partial x'_l \partial x_n}\right)\boldsymbol{n}_j\,\mathrm{d}S(\mathbf{y}) \\ &+\int_{V}\frac{\partial \boldsymbol{G}^{\infty}_{im}(x,x')}{\partial x'_l \partial x_n}\left(\boldsymbol{b}^{\mathrm{M}}_{ijkl} - \boldsymbol{b}_{ijkl}\right)\dot{\boldsymbol{\varepsilon}}^{\mathrm{vp}}_{kl}(x')\mathrm{d}V(x')\end{aligned} \tag{14}$$

The expression of the local strain rate tensor is derived from Eq. (14) via use of the compatibility condition:

$$\begin{aligned}\dot{\boldsymbol{\varepsilon}}^{\mathrm{vp}}_{ij}(x) = &T_{ijmn}\left(\boldsymbol{b}^{\mathrm{M}}\right)\left(\boldsymbol{b}^{\mathrm{M}}_{mnkl} - \boldsymbol{b}^{\mathrm{I}}_{mnkl}\right)\dot{\boldsymbol{\varepsilon}}^{\mathrm{vpI}}_{kl} \\ &+\int_{S}\boldsymbol{b}^{\mathrm{M}}_{mnkl}\Delta\dot{\boldsymbol{u}}_k(x')\Gamma^{\infty}_{ijmn}(x',x)\boldsymbol{n}_l\,\mathrm{d}S(x').\end{aligned} \tag{15}$$

Here $\boldsymbol{T}(\boldsymbol{b}^{\mathrm{M}})$ denotes the interaction tensor given by $\boldsymbol{T}\left(\boldsymbol{b}^{\mathrm{M}}\right) = \int_{\boldsymbol{\Omega}}\Gamma^{\infty}(x,x')\,\mathrm{d}x'$, where $\Gamma^{\infty}_{ijkl}(x,y)$ denotes Green's modified operator. Eq. (15) can be further developed by introducing the time derivative of the displacement jump condition given by Eq. (2). Note that the time derivative of the displacement jump will introduce the time derivative of the stress tensor, which is supposed here to be negligible compared to that of the interface compliance tensor. Hence one obtains

$$\begin{aligned}\dot{\boldsymbol{\varepsilon}}^{\mathrm{vp}}_{ij}(x) = &T\left(\boldsymbol{b}^{\mathrm{M}}_{mnpq}\right)\left(\boldsymbol{b}^{\mathrm{M}}_{pqkl} - \boldsymbol{b}^{\mathrm{I}}_{pqkl}\right)\dot{\boldsymbol{\varepsilon}}^{\mathrm{vpI}}_{kl} \\ &+\int_{S}\boldsymbol{b}^{\mathrm{M}}_{mnkl}\dot{\eta}_{kp}\boldsymbol{\sigma}_{pq}\boldsymbol{n}_q\Gamma^{\infty}_{ijmn}(x',x)\boldsymbol{n}_l\,\mathrm{d}S(x').\end{aligned} \tag{16}$$

In order to pursue the analytical developments, the stress state along the interface is supposed constant and equal

to the stress state in the inclusion. Hence, introducing the constitutive law in the inclusion into Eq. (16) and averaging the resulting equation on the inclusion's volume, one obtains

$$\dot{\boldsymbol{\varepsilon}}_{ij}^{\mathrm{vpI}} = T_{ijpq}\left(\boldsymbol{b}^{\mathrm{M}}\right)\left(\boldsymbol{b}_{pqkl}^{\mathrm{M}} - \boldsymbol{b}_{pqkl}^{\mathrm{I}}\right)\dot{\boldsymbol{\varepsilon}}_{kl}^{\mathrm{vpI}} + \dot{\boldsymbol{\varepsilon}}_{ab}^{\mathrm{vpI}}\boldsymbol{b}_{pqab}^{\mathrm{I}}\boldsymbol{b}_{mnkl}^{\mathrm{M}}T_{ijmn}\left(\boldsymbol{b}^{\mathrm{M}}\right)\int_S \dot{\eta}_{kp}\boldsymbol{n}_q\boldsymbol{n}_l\,\mathrm{d}S(x') + \dot{\boldsymbol{\varepsilon}}_{ij}^{\mathrm{vpM}}. \tag{17}$$

Note here that the third term on the right-hand side of Eq. (17) results from the boundary conditions. Let us approximate the above integral by its average value. Hence, one obtains

$$\dot{\boldsymbol{\varepsilon}}_{ij}^{\mathrm{vpI}} = T_{ijpq}\left(\boldsymbol{b}^{\mathrm{M}}\right)\left(\left(\boldsymbol{b}_{pqkl}^{\mathrm{M}} - \boldsymbol{b}_{pqkl}^{\mathrm{I}}\right) + \boldsymbol{b}_{pqab}^{\mathrm{M}}\boldsymbol{R}_{abmn}\boldsymbol{b}_{mnkl}^{\mathrm{I}}\right)\dot{\boldsymbol{\varepsilon}}_{kl}^{\mathrm{vpI}} + \dot{\boldsymbol{\varepsilon}}_{ij}^{\mathrm{vpM}}, \tag{18}$$

where $\boldsymbol{R}$ is given by

$$\boldsymbol{R}_{mnpq} = \frac{1}{4\Omega_{\mathrm{I}}} \times \int_S \left(\dot{\eta}_{mp}\boldsymbol{n}_q\boldsymbol{n}_n + \dot{\eta}_{mq}\boldsymbol{n}_p\boldsymbol{n}_n + \dot{\eta}_{np}\boldsymbol{n}_q\boldsymbol{n}_m + \dot{\eta}_{nq}\boldsymbol{n}_p\boldsymbol{n}_m\right)\mathrm{d}S(x'). \tag{19}$$

Note here that in the case of a simple expression of the interface compliance, an analytical expression of tensor $\boldsymbol{R}$ can be obtained. Eq. (18) can be written as follows:

$$\dot{\boldsymbol{\varepsilon}}_{ij}^{\mathrm{vpI}} = \boldsymbol{B}_{ijkl}^{\mathrm{vpI}}\dot{\boldsymbol{\varepsilon}}_{kl}^{\mathrm{vpM}}, \tag{20}$$

where $\boldsymbol{B}^{\mathrm{vpI}}$ denotes the localization tensor given by

$$\boldsymbol{B}_{ijkl}^{\mathrm{vpI}} = \left[I_{ijkl} - T_{ijpq}\left(\boldsymbol{b}^{\mathrm{M}}\right)\left(\left(\boldsymbol{b}_{pqkl}^{\mathrm{M}} - \boldsymbol{b}_{pqkl}^{\mathrm{I}}\right) + \boldsymbol{b}_{pqab}^{\mathrm{M}}\boldsymbol{R}_{abmn}\boldsymbol{b}_{mnkl}^{\mathrm{I}}\right)\right]^{-1}. \tag{21}$$

Finally step 1 is concluded via the Mori–Tanaka approximation, which leads to the following expression of the overall viscosity tensor $\boldsymbol{b}^{\mathrm{HI}}$:

$$\boldsymbol{b}^{\mathrm{HI}} = (1-f)\boldsymbol{b}^{\mathrm{M}} + f\boldsymbol{b}^{\mathrm{I}} : \boldsymbol{A}^{\mathrm{vpI}}. \tag{22}$$

Here f denotes the inclusion's volume fraction. The previous set of equations (e.g. Eqs. (20)–(22)) provides a complete solution to the first step of the development. In the second step of the framework, the HI is introduced in a medium representative of the overall material. The interface between the HI and the effective material is assumed perfect. Hence, one obtains the localization expressions given by

$$\dot{\boldsymbol{\varepsilon}}_{ij}^{\mathrm{vpHI}} = \boldsymbol{B}_{ijkl}^{\mathrm{vpHI}}\dot{\boldsymbol{E}}_{kl}^{\mathrm{vp}}. \tag{23}$$

Here $\dot{\boldsymbol{E}}^{\mathrm{vp}}$ denotes the macroscopic viscoplastic strain rate tensor and the localization tensor is given by

$$\boldsymbol{B}_{ijkl}^{\mathrm{vpHI}} = \left(I_{ijkl} - T_{ijpq}\left(\boldsymbol{b}^{\mathrm{e}}\right)\left(\boldsymbol{b}_{pqkl}^{\mathrm{e}} - \boldsymbol{b}_{pqkl}^{\mathrm{HI}}\right)\right)^{-1}, \tag{24}$$

where $\boldsymbol{b}^{\mathrm{e}}$ denotes the effective viscosity tensor. From the solutions of steps 1 and 2 the overall localization relation can be derived. Precisely, combining the macrohomogeneity condition of step 1 and the two localization relations given by Eqs. (23) and (20), one obtains the following localization relation:

$$\dot{\boldsymbol{\varepsilon}}^{\mathrm{vpI}} = \boldsymbol{B}^{\mathrm{I}} : \dot{\boldsymbol{E}}^{\mathrm{vp}}, \tag{25}$$

where the overall viscoplastic localization tensor is given by

$$\boldsymbol{B}^{\mathrm{I}} = \left[(1-f')\left(\boldsymbol{B}^{\mathrm{vpHI}}\right)^{-1} : \left(\boldsymbol{B}^{\mathrm{vpI}}\right)^{-1} + f'\left(\boldsymbol{B}^{\mathrm{vpHI}}\right)^{-1}\right]^{-1}. \tag{26}$$

Here f' denotes the volume fraction of the homogenized inclusion. From the localization relation in the above, the viscoplastic problem can be completely solved. The solution to the purely viscoplastic problem can be extended to the case of elastoviscoplastic solutions via the use of the field translation method introduced in work by Sabar. For the sake of conciseness the field translation framework will not be repeated here. Hence, the overall elastoviscoplastic localization relation is given by

$$\dot{\boldsymbol{\varepsilon}}^{\mathrm{I}} = \boldsymbol{A}^{\mathrm{I}} : \left(\dot{\boldsymbol{E}} - \dot{\boldsymbol{E}}^{\mathrm{vpe}}\right) + \boldsymbol{A}^{\mathrm{I}} : \boldsymbol{B}^{\mathrm{I}} : \dot{\boldsymbol{E}}^{\mathrm{vp}} + \boldsymbol{A}^{\mathrm{I}} : \boldsymbol{S}^{\mathrm{E}} : \boldsymbol{S}^{\mathrm{e}} : \left(\boldsymbol{c}^{\mathrm{I}} : \dot{\boldsymbol{\varepsilon}}^{\mathrm{vpI}} - \boldsymbol{C}^{\mathrm{e}} : \boldsymbol{B}^{\mathrm{I}} : \dot{\boldsymbol{E}}^{\mathrm{vp}}\right). \tag{27}$$

For the sake of simplicity, let us assume that the averaged local viscoplastic strain rate can still be related with Eq. (25). Similarly, the averaged local elastic strain rates can be related via the equivalent to Eq. (25) in the case of pure elastic behavior. Hence, $\boldsymbol{A}^{\mathrm{I}}$ represents the elastic equivalent of the localization tensor $\boldsymbol{B}^{\mathrm{I}}$. However, let us note that another interface condition must be introduced to describe the contribution of imperfect interface bonding to the elastic deformation. Also, $\boldsymbol{C}^{\mathrm{e}}$, $\boldsymbol{c}^{\mathrm{I}}$, $\boldsymbol{S}^{\mathrm{e}}$, $\boldsymbol{S}^{\mathrm{E}}$ denote the macroscopic elasticity tensor, the local elasticity tensor in the inclusion phase, the overall compliance tensor and Eshelby's tensor [24], respectively. Hence, a complete solution can be found in the case of elastoviscoplasticity.

3. Application to nanocrystalline materials

The hierarchal scale transition framework presented in the above was applied to simulate the size effect in pure face-centered cubic copper polycrystals in which imperfect phase bonding is expected to occur when the crystallite size lies in the nanometer range. This may lead to damage that limits the ductility of the material. As a first approach the present study is limited to the onset of relative sliding of grains, and void creation is not accounted for. In a continuation of previous work by the authors [15], the model will be applied solely in the viscoplastic case. The inclusion phase will represent grain interiors and the coating phase will represent grain boundaries and triple junctions. Both phases are assumed isotropic.

Viscoplastic deformation in crystallites with sizes larger than ~30–50 nm occurs – in the quasi-static range – via the thermally activated glide of dislocation. Dislocation mobility is hindered by the stress fields resulting from the presence of grain boundaries and of sessile dislocations

[25–27]. The stored dislocation density evolves via the athermal dislocation storage mechanism and the thermally activated dislocation annihilation mechanism [28,29]. When the grain size is smaller than ~30–50 nm, experiments report severely reduced stored dislocation density [30] and dislocation storage, and annihilation may not be activated. Simultaneously, it was suggested via molecular dynamics simulation and transmission electron microscopy that grain boundaries act as dislocation sources [30–32]. The emission of dislocations from grain boundaries will have two effects: (i) local atomic reorganization within the grain boundary and (ii) deformation within the grain interior following the glide of an emitted dislocation.

The viscoplastic response of the crystallites – represented by the inclusion phase – accounts for the thermally activated glide of dislocations described by a power law [17]:

$$\dot{\boldsymbol{\varepsilon}}_{\mathrm{eq}}^{\mathrm{vpI}} = \dot{\boldsymbol{\varepsilon}}_0 \left(\frac{\boldsymbol{\sigma}_{\mathrm{eq}}^{\mathrm{I}}}{\boldsymbol{\sigma}_{\mathrm{f}}} \right)^m. \tag{28}$$

Here $\dot{\boldsymbol{\varepsilon}}_{\mathrm{eq}}^{\mathrm{vpI}}$ denotes the equivalent viscoplastic strain rate within the inclusion phase. $\boldsymbol{\sigma}_{\mathrm{eq}}^{\mathrm{I}}$, $\dot{\boldsymbol{\varepsilon}}_0$, m, $\boldsymbol{\sigma}_{\mathrm{f}}$ denote the equivalent stress in the inclusion phase, a reference strain rate, the flow exponent and the flow stress at 0 K, respectively. The flow stress at 0 K accounts for the contributions of the stored dislocations and the grain boundaries:

$$\boldsymbol{\sigma}_{\mathrm{f}} = \alpha M G \boldsymbol{b} \sqrt{\rho} + \beta / \sqrt{d}. \tag{29}$$

Here α is a constant. G, M, ρ, $\boldsymbol{b}$, β and d, respectively, denote the shear modulus, the Taylor factor, the dislocation density, the magnitude of the Burgers vector, the Hall–Petch slope and the grain size. The dislocation density evolves via athermal storage – resulting in a decrease in the mean free path of mobile dislocations – and via dynamic recovery:

$$\frac{\mathrm{d}\rho}{\mathrm{d}\boldsymbol{\varepsilon}_{\mathrm{eq}}^{\mathrm{vpI}}} = M \left(\frac{k_0}{d} + k_1 \sqrt{\rho} - k_{20} \left(\frac{\dot{\boldsymbol{\varepsilon}}_{\mathrm{eq}}^{\mathrm{vpI}}}{\dot{\boldsymbol{\varepsilon}}_*} \right)^{-1/n} \rho \right). \tag{30}$$

Here k_0, k_1 and k_{20} are three parameters controlling the rate of storage and annihilation of dislocations. As mentioned in the above, in the case of crystallites smaller than ~30 nm, dislocation annihilation and storage may not be activated. Therefore, below this grain size, the dislocation density evolution will be deactivated in a set of simulations.

Grain boundaries and triple junctions, represented by the matrix phase, are assumed to deform via the combined activity of grain boundary dislocation emission and penetration, for which a constitutive law was introduced by the authors. It is assumed that grain boundary dislocation emission, which is know to be thermally activated, triggers the dislocation penetration mechanism, which leads to a net strain within the grain boundary opposite to the source. In other words, consistent with molecular dynamics simulations, it is assumed that every emitted dislocation ends its trajectory in the grain boundary opposite the source. The equivalent viscoplastic strain rate in the matrix phase is given by [17]

$$\dot{\boldsymbol{\varepsilon}}_{\mathrm{eq}}^{\mathrm{vpC}} = \frac{\chi}{d^3} \left(\frac{\boldsymbol{\sigma}_{\mathrm{eq}}^{\mathrm{I}}}{\boldsymbol{\sigma}_{\mathrm{c}}^{\mathrm{I}}} \right)^m \exp\left(-\frac{\Delta G_0}{k_{\mathrm{B}} T} \left(1 - \left(\frac{\boldsymbol{K} \cdot \boldsymbol{\sigma}_{\mathrm{eq}}^{\mathrm{C}}}{\boldsymbol{\sigma}_{\mathrm{c}}^{\mathrm{M}}} \right)^p \right)^q \right). \tag{31}$$

Here $d, \boldsymbol{\sigma}_{\mathrm{eq}}^{\mathrm{I}}$, $\boldsymbol{\sigma}_{\mathrm{c}}^{\mathrm{I}}$, m, k_{B}, T, $\boldsymbol{\sigma}_{\mathrm{eq}}^{\mathrm{C}}$, p and q represent the grain diameter, the Von Mises stress in the grain core, the grain core flow stress at 0 K, the flow exponent, the Boltzmann constant, the absolute temperature (K), the Von Mises stress in the matrix phase, and two coefficients that characterize the shape of the dislocation emission resistance curve, respectively. The critical emission stress at 0 K and the free enthalpy of activation are represented by $\boldsymbol{\sigma}_{\mathrm{c}}^{\mathrm{M}}$ and ΔG, respectively. These two parameters are extracted from molecular dynamics simulations of stepped bicrystal interfaces. $\boldsymbol{K}$ denotes a stress heterogeneity factor which compensates for the limitations of the micromechanical scheme used in this work which is limited to homogeneous states of stress and strains within each phase. Moreover, these stress and strain heterogeneities were predicted in several models. In the previous equation, χ is given by

$$\chi = \frac{m_{\mathrm{dis}} v_0 \delta \sin(\theta)}{(m_{\mathrm{dis}} + m_{\mathrm{GB}}) l} \tag{32}$$

Here m_{dis}, m_{GB}, v_0, δ, θ and t represent the average dislocation rest mass, the interface mass affected by a dislocation absorption event, the ledge density per unit area, the dislocation emission angle and a numerical constant, respectively.

Finally, the constitutive law presented in the above and the scale transition framework combined with the proposed interface conditions (e.g. Eq. (4)) were implemented to simulate the size effect in copper. Precisely, the tensile response of nanometer and conventional copper representative volumes was simulated for several grain sizes. Note that this model allows the prediction, in a qualitative manner since elasticity is not considered, of the coupled activity of grain boundary sliding and grain boundary dislocation emission and penetration.

The parameters that are used are given in Table 1. All parameters related to the inclusion phase and the matrix phase are extracted from Refs. [16,17]. In the case of the interface, the critical debonding length δ_{c} was varied from 1 to 3 nm, which corresponds approximately to ~3–10 interatomic distances. Since grain boundary sliding can be localized in grain boundaries as well as triple junctions, a simple rule of mixture was used to estimate the critical sliding stress. Since triple junctions are known to exhibit a structure devoid of any particular order, similar to an amorphous structure, its critical sliding stress is estimated to be equal to the yield stress of a hypothesized amorphous copper material. w in Table 1 refers to the grain boundary thickness. Note that as opposed to previous work by the authors, the free enthalpy of activation and the critical emission stress are calculated via molecular simulations [9].

Table 1
Model parameters

Inclusion phase	$m = 230$	$n = 21.25$	$\alpha = 0.33$	$M = 3.06$
	$\boldsymbol{b} = 0.257$ nm	$\beta = 0.11$ Mpa m$^{-1/2}$	$k = 3.9E9$ m^{-1}	$k_1 = 1.E10$ m^{-1}
	$k_{20} = 330$	$\dot{\varepsilon}_* = 1/s$	$\dot{\varepsilon}_0 = 0.005/s$	$\mu^{\mathrm{I}} = 38$ GPa
Matrix phase	$\dot{m}_{\mathrm{dis}} = 3.15$ pN ps^2/Å^2	$\delta = 40$	$v_0 = 0.03$	$l = 1/2$
	$m_{\mathrm{GB}} = \pi \cdot \frac{w^2}{4} \cdot l \cdot \rho_{\mathrm{GB}}$	$\rho_{\mathrm{GB}} = 7.61$ g/cm^3	$\mu^{\mathrm{M}} = 30$ GPa	$w = 1$ nm
	$\Delta G_0 = 103.8$ mJ/m^2	$\boldsymbol{\sigma}_{\mathrm{c}}^{\mathrm{M}} = 2450$ MPa	$p = 1$	$q = 1.5$
Interface	$\delta_{\mathrm{c}} = 1, 2, 3$ nm	$\boldsymbol{\sigma}_{\mathrm{c}}^{\mathrm{TJ}} = 800$ *MPa*		

In order not to overestimate the effect of grain boundaries and triple junctions, the volume fractions of the inclusions in steps 1 and 2 are different. Precisely, in the first step the matrix phase represents only half the volume fraction of the grain boundaries and triple junctions predicted with a spherical grain assumption. Consequently in step 1, the volume fraction of the inclusion, denoted f (the volume fraction of matrix is equal to $1-f$), is given by

$$f = \left(\frac{d}{d + w/2}\right)^3. \tag{33}$$

However, in step 2 the volume fraction of the inclusion, denoted f' (the volume fraction of the HEM is equal to $1-f'$), is given by

$$f' = \left(\frac{d + w/2}{d + w}\right)^3. \tag{34}$$

Finally, the critical sliding stress, denoted $\boldsymbol{\sigma}_{\mathrm{c}}$ in Eq. (4), is taken as the mixture rule between the critical grain boundary stress $\boldsymbol{\sigma}_{\mathrm{c}}^{\mathrm{M}}$ and the critical triple junction stress $\boldsymbol{\sigma}_{\mathrm{c}}^{\mathrm{TJ}}$. Nanocrystalline materials exhibit numerous size effects, such as size-dependent strain rate sensitivity and "abnormal" evolution of the yield stress with the grain size characterized by the breakdown of the Hall–Petch law [33,34] resulting from the activity of mechanisms not operating in the conventional regime. The two most probable mechanisms which were suggested to result in the breakdown of the Hall–Petch law are (i) grain boundary sliding and (ii) grain boundary dislocation emission [35–37].

As shown in a previous study, the mechanism of grain boundary dislocation emission can result in a softening in the viscoplastic response of nanocrystalline materials. However, the activation of grain boundary dislocation emission requires the presence of large states of stress within the grain boundaries. When the stress heterogeneity factor, K, is equal to 1, grain boundary dislocation emission is severely limited, if not inactive, and one would expect the abnormal grain boundary sliding to be the primary softening mechanism. This can be observed in Fig. 3, which shows the evolution of the yield stress with respect to the inverse of the square root of the grain size. The dark bold curve corresponds to the case where grain boundary sliding is activated, while the dark dashed curve corresponds to the case where grain boundary sliding is deactivated. The red[1] curves correspond to plots of the Hall–Petch law for two different initial states of stress in the conventional regime. The stress heterogeneity factor was set to 1 in these simulations. Hence, the effect of grain boundary dislocation emission is negligible. On the one hand, when grain boundary sliding is not allowed, no remarkable breakdown of the Hall–Petch law is predicted. However, let us note that a Hall–Petch slope slightly lower than that measured experimentally is predicted. On the other hand, one can observe that grain boundary sliding, modeled here as a stick slip mechanism, leads to a noticeable breakdown of the Hall–Petch law. Hence, the model predicts that the sole activity of grain boundary sliding is sufficient to lead to the observed softening in the viscoplastic response of nanocrystalline materials.

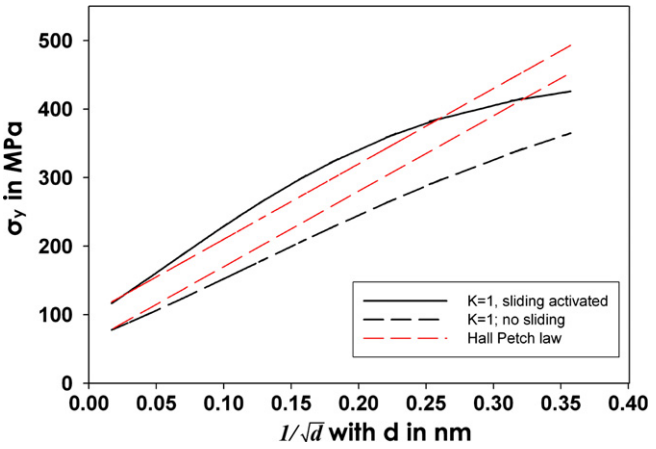

Fig. 3. Effect of grain boundary sliding on the evolution of yield stress with grain size.

Fig. 4 shows the tensile response of 15 nm grain nanocrystalline copper for three values of the critical debonding length δ_{c} (1, 2 and 3 nm). Let us remark that the effect of the debonding length on the overall model prediction is negligible in the possible range of values of the parameter.

As discussed above, in the nanocrystalline regime, the activity of dislocations within grain interiors – in terms of storage and annihilation – is expected to be negligible.

[1] For interpretation of color in Fig. 3, the reader is referred to the web version of this article.

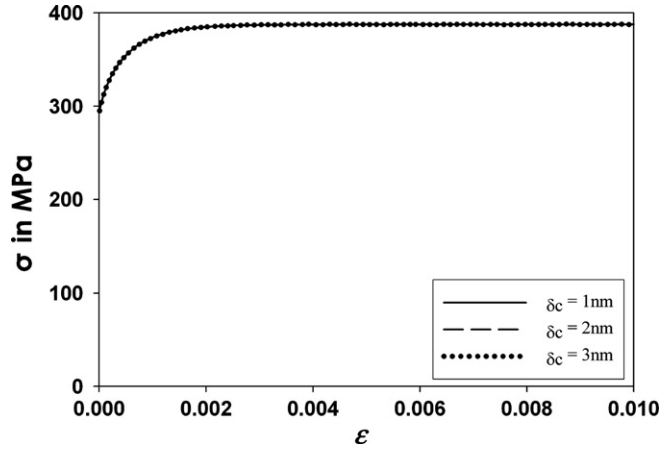

Fig. 4. Effect of grain critical debonding length on the macroscopic tensile response of 15 nm grain nanocrystalline copper.

Hence, in Fig. 3 and in previous analyses by the authors and others, the response of grain interiors is clearly overestimated. The effect of this assumption is presented in Fig. 5 which shows the evolution of yield stress with the inverse of the square root of the grain size in the case where dislocation activity is not prevented (bold curve) and in the case where dislocation evolution is deactivated for grain sizes smaller than 30 nm (dashed curve). The stress heterogeneity factor, K, was set to 1. Hence, grain boundary dislocation emission is negligible. One can observe that upon deactivating the dislocation evolution, the yield stress decreases sharply with a decrease in the grain size prior to increasing again with a reduced Hall–Petch slope. The sharp decrease is an artifact resulting from the fact that when dislocation activity is prevented, the response of the inclusion phase becomes elastic–perfectly plastic. Therefore, the grain interiors present no hardening, resulting in this sharp decrease. However, one can observe that, disregarding the offset in the two curves, the slopes remain equal, independent of the activity of dislocations. Hence, it is shown here that models accounting for dislocation storage and annihilation within the nanocrystalline regime clearly overestimate the response of grain interiors and, consequently, the overall response. Hence, no quantitative conclusion can be drawn from such models. However, as shown in Fig. 5, qualitative analysis can still be performed from these approximated models.

The simultaneous effect of grain boundary sliding and grain boundary dislocation emission is presented in Fig. 6, which shows the evolution of the yield strength with the inverse of the square root of the grain size. In these simulations, dislocation evolution is allowed within the grain interiors. Three cases are presented, corresponding to stress heterogeneity factors K=1, 1.5 and 2, represented by the bold, dashed and dotted curves, respectively. One can observe that the softening in the viscoplastic response of nanocrystalline materials, characterized by the breakdown of the Hall–Petch law, becomes more pronounced with an increase in the stress heterogeneity factor. This results from the fact that an increase in the stress heterogeneity factor results in an increase in the activity of grain boundary dislocation emission. One can observe in Fig. 7, which presents predictions of the tensile response of 15 nm grain nanocrystalline copper in the cases where the stress heterogeneity factor, K, is set to 1, 1.5 and 2, that the activity of grain boundary dislocation emission results in a softening in the viscoplastic response of nanocrystalline materials.

From the above figures, it can be seen that the proposed model allows the prediction of the simultaneous, and implicitly coupled, activity of grain boundary sliding and grain boundary dislocation emission. Among other things, one can conclude that the breakdown of the Hall–Petch law should be more pronounced in the case of nanocrystalline materials presenting highly irregular grain boundaries. Hence, this should apply to nanocrystalline materials fabricated by severe plastic deformation, which have been shown to exhibit highly stepped grain boundaries [38]. Similarly, nanocrystalline materials with less irregular grain boundaries will deform viscoplastically via grain boundary

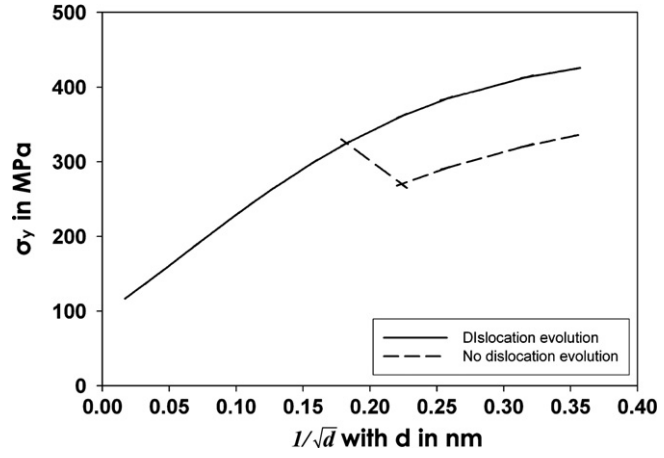

Fig. 5. Effect of intragranular dislocation activity on the evolution of yield stress with the grain size.

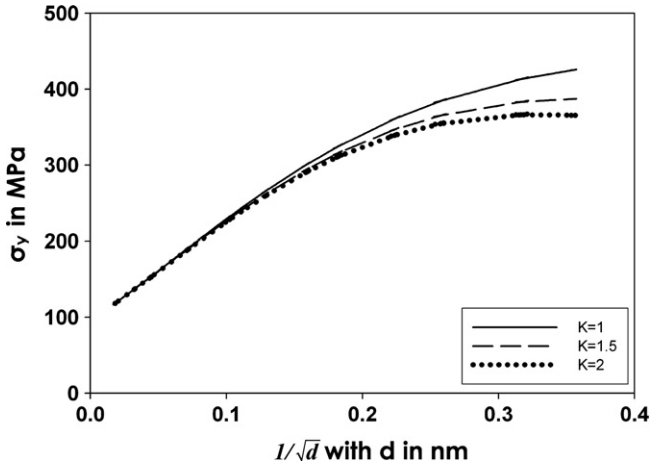

Fig. 6. Coupled effect of grain boundary dislocation emission and grain boundary sliding on the evolution of yield stress with the grain size.

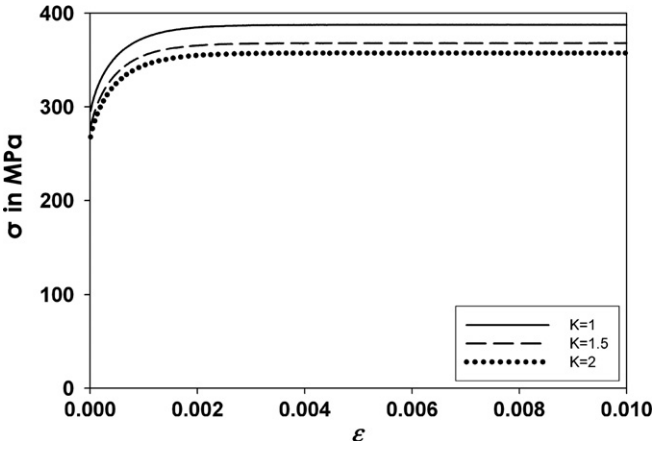

Fig. 7. Effect of grain boundary dislocation emission on the macroscopic tensile response of 15 nm grain nanocrystalline copper.

sliding. In the case of an accommodation of grain boundary sliding via vacancy diffusion, the material's ductility is not then prejudiced by the activity of grain boundary sliding. However, in the case where vacancy diffusion is not activated, or where it is activated at a rate not sufficient to accommodate grain boundary sliding, the deformation of nanocrystalline materials will be followed by void creation within the material. This case will be the subject of future study. Also, it was shown that the grain size distribution and related variance has a non-negligible influence on the response of nanocrystalline materials [39]. This feature will be added to the present model.

4. Conclusion

A hierarchal scale transition framework was introduced to allow the prediction of the overall elastoviscoplastic response of composite materials with imperfect interfaces. The homogenization procedure relies on the decomposition of a three-phase material's representation into two two-phase problems. First the viscoplastic response of a representative volume element composed of the two imperfectly bonded phases is predicted via the introduction of interface conditions and via the Mori–Tanaka approximation. Second, the homogenized material is embedded in a matrix with effective properties and the overall viscoplastic response is predicted with the self-consistent approximation. Finally the overall elastoviscoplastic behavior is obtained via the field translation method. The model was applied to the case of pure nanocrystalline copper for which both the activity of dislocation glide, grain boundary dislocation emission and grain boundary sliding were considered. The relative sliding of grain interiors was modeled as a stick–slip mechanism where the compliance of the interface varies during deformation. It was shown that the present framework allows the prediction of the simultaneous activity of grain boundary dislocation emission and grain boundary sliding. The former is expected to be predominant in the case of nanocrystalline materials with a high content of largely non-uniform grain boundaries, while the latter is expected to be predominant in the case of nanocrystalline materials with a high content of uniform grain boundaries. Further study will investigate the mechanism of void creation and the effect of grain size distribution.

References

[1] Gleiter H. Acta Mater 2000;48:1–29.
[2] Kumar KS, Suresh S, Chisolm MF, Horton JA, Wang P. Acta Mater 2003;51:387–405.
[3] Warner DH, Sansoz F, Molinari JF. Int J Plasticity 2006;22(4):754–74.
[4] Zener C. Phys Rev 1941;60:906–8.
[5] Langdon TG. Phil Mag 1970;22:689–700.
[6] Wu XJ, Koul AK. Metall Mater Trans 1994;26:905–14.
[7] Wu XJ, Koul AK. Adv Perf Mater 1997;4:409–20.
[8] Raj R, Ashby MF. Metall Trans 1971;2:1113–27.
[9] Mori T, Huang JH, Taya M. Acta Mater 1997;45:429–38.
[10] Onaka S, Huang JH, Wakashiima K, Mori T. Acta Mater 1998;46:3821–8.
[11] Wei YJ, Anand L. J Mech Phys Sol 2004;52(11):2587–616.
[12] Mori T, Tanaka K. Acta Metall 1973;21(5):571–4.
[13] Berbenni S, Favier V, Lemoine X, Berveiller M. Mater Sci Eng A 2004;372:128–36.
[14] Sabar H, Berveiller M, Favier V, Berbenni S. Int J Sol Struct 2002;39(12):3257–76.
[15] Benkassem S, Capolungo L, Cherkaoui M. Acta Mater 2007;55(10):3563–72.
[16] Capolungo L, Spearot DE, Cherkaoui M, McDowell DL, Qu J, Jacob KI. J Mech Phys Sol 2007;55(11):2300–27.
[17] Capolungo L, Cherkaoui M, Qu J. Int J Plasticity 2007;23(4):561–91.
[18] Christensen RM, Lo KH. J Mech Phys Sol 1979;27:315–30.
[19] Cherkaoui M, Sabar H, Berveiller M, 9th French National Colloquium on Composite Materials. Compos Sci Technol 1996;56(7):877–82.
[20] Hill R. J Mech Phys Sol 1983:31.
[21] Hadamard J. Leçons sur la propagation des ondes et les equations de l'hydrodynamique. Paris: A. Hermann; 1903.
[22] Qu J. Mech Mater 1993;14(4):269–81.
[23] Qu J. J Appl Mech Trans ASME 1993;60(4):1048–50.
[24] Eshelby JD. Proc Roy Soc Lond A 1957;241:376–96.
[25] Estrin Y, Mecking H. Acta Metall 1984;32:57–70.
[26] Kocks UF. Trans ASME 1976:76–85.
[27] Kocks UF, Argon AS, Ashby MF. Prog Mater Sci 1975;19:1–291.
[28] Nes E. Prog Mater Sci 1997;41:129–93.
[29] Stokes RJ, Cottrel AH. Acta Metall 1954:2.
[30] Langlois C, Hytch MJ, Lartigue-Korinek S, Champion Y. Metall Mater Trans 2005;36:3451.
[31] Van Swygenhoven H, Caro A, Farkas D. Scripta Mater 2001;44:1513–6.
[32] Wolf D, Yamakov V, Phillpot SR, Mukherjee A, Gleiter H. Acta Mater 2005;53:1–40.
[33] Hall EO. Proc Roy Soc Lond B 1951;64:747.
[34] Petch NJ. J Iron Steel Inst 1953;74:25.
[35] Froseth AG, Derlet PM, Van Swygenhoven H. Acta Mater 2004;52:5863–70.
[36] Malis T, Tangri K. Acta Metall 1979;27:25–32.
[37] Yamakov V, Wolf D, Slalzar M, Phillpot SR, Gleiter H. Acta Mater 2001;49:2713–22.
[38] Huang JY, Liao XZ, Zhu YT, Zhou F, Lavernia EJ. Phil Mag 2003;83(12):1407–19.
[39] Berbenni S, Favier V, Berveiller M. Comp Mater Sci 2007;39(1):96–105.